

Performance of Corrosion-Resistant Alloys in Concentrated Acids

Ajit Mishra¹

Received: 16 August 2016/Revised: 31 October 2016/Published online: 13 February 2017
© The Chinese Society for Metals and Springer-Verlag Berlin Heidelberg 2017

Abstract Nickel alloys containing optimum amounts of chromium (Cr), molybdenum (Mo) and tungsten (W) are widely used in the chemical processing industries due to their tolerance to both oxidizing and reducing conditions. Unlike stainless steel (SS), Ni–Cr–Mo (W) alloys exhibit remarkably high uniform corrosion resistance in major concentrated acids, like hydrochloric acid (HCl) and sulfuric acid (H₂SO₄). A higher uniform corrosion resistance of Ni–Cr–Mo (W) alloys, compared to other alloys, in concentrated acids can be attributed to the formation of protective oxide film of Mo and W in reducing acids, and Cr oxide film in oxidizing solutions. The localized corrosion resistance of Ni–Cr–Mo (W) alloys, containing high amount Cr as well as Mo (or Mo + W), is also significantly higher than that of other commercially available alloys. The present study investigates the role of alloying elements, in nickel alloys, to uniform corrosion resistance in concentrated acids (HCl, HCl + oxidizing impurities and H₂SO₄) and localized corrosion performance in chloride-rich environments using ASTM G-48 test methodology. The corrosion tests were conducted on various alloys, and the results were analyzed using weight loss technique and electrochemical techniques, in conjunction with surface characterization tools.

KEY WORDS: Nickel–chromium–molybdenum–tungsten; Corrosion-resistant alloys; Reducing acid; Oxidants; Localized corrosion; Surface characterization

1 Introduction

Chemical processing environments vary greatly so materials selection is a complex topic. However, it can be simplified by understanding the role of alloying elements, both individual and in synergy, added in an optimum concentration in an alloy to its corrosion performance in aggressive environments. Also, a better knowledge of the solution chemistry can assist the end users to focus on

materials that may potentially meet the requirements of the application. While the list of corrodents in the chemical processing industries (CPI) is endless, many fall into some general categories such as acidic, basic, reducing or oxidizing. The present study focuses on the materials performance in concentrated sulfuric acid (H₂SO₄) and hydrochloric acid (HCl).

Sulfuric acid is one of the world's most important industrial chemicals as it is used in a variety of industrial processes. It is the largest tonnage heavy industrial chemical manufactured. Sulfuric acid is used in phosphate fertilizer production, paper industry, lead-based batteries for vehicles, purification of petroleum, pickling of metals, electroplating bath, production of rayon and film, and as a laboratory reagent [1].

Hydrochloric acid (HCl) is another important mineral acid, second only to sulfuric acid (H₂SO₄) in its uses in

Available online at <http://link.springer.com/journal/40195>

✉ Ajit Mishra
ajitosu@gmail.com

¹ Research and Technology, Haynes International, 1020 Park Ave, Kokomo, IN 46902, USA

industry. Major applications include acid pickling of steel, acid treatment of oil wells, chemical cleaning and processing, ore reduction, production of chlorine and chlorides and food processing [2]. There is a very limited choice of materials for use in HCl solution, as most of the commonly used metals and their alloys experience extensive general and/or localized corrosion attack in the HCl. The solution aggressiveness drastically changes depending upon the concentration, temperature and the presence of oxidizing impurities (like ferric ions and cupric ions) [3].

Nickel-based metals, alloyed with Cr, Mo, W and other elements, are widely used in concentrated acidic solutions because of their excellent corrosion resistance in both oxidizing and reducing environments [4]. The presence of sufficient Cr in Ni alloys enforces the growth of a passive barrier oxide layer of Cr₂O₃ on the surface, and Mo and W retard the propagation of localized corrosion if the passive film is breached [5–8]. Therefore, optimization of the concentration of Cr, Mo and W is the key feature in developing Ni–Cr–Mo and Ni–Cr–Mo–W alloys, which are resistant to uniform and localized corrosion and stress corrosion cracking [4].

In past, an extensive study was conducted on the performance of Ni–Cr–Mo (W) alloys in concentrated HCl acid using weight loss technique and an iso-corrosion curve was generated for various corrosion-resistant Ni-based alloys [4]. However, the study was confined up to 20 wt% HCl acid, whereas the maximum concentration of reagent grade HCl acid is 37 wt%. Meck et al. [9] further studied the corrosion performance of B-3[®] and C-2000[®] alloys in 20 wt% reagent grade HCl acid, with and without the presence of impurities, using an electrochemical technique. In the reagent grade HCl solution, B-3 alloy demonstrated a high corrosion resistance. However, in the presence of oxidizing impurity, the corrosion resistance of C-2000 alloy was significantly higher compared to B-3 alloy. The results are in consensus with the weight loss data [4]. Recently, Mishra et al. [10] demonstrated the role of alloying elements on the corrosion performance of various Ni–Cr–Mo (W) alloys in aggressive chloride environment which can also be simulated as a critical crevice solution.

In the present study, an attempt was made to generate an iso-corrosion curve for various corrosion-resistant alloys in HCl acid up to 37 wt% (maximum reagent grade concentration) using weight loss technique. Furthermore, the study utilized electrochemical techniques and characterization tools to investigate the role of alloying elements on the corrosion performance of alloys in HCl acid, with and without the presence of oxidants. Similar to corrosion study in HCl acid, experiments were conducted in various concentrations and temperatures of H₂SO₄ acid and the results were analyzed using multiple techniques. The major focus of present study is not to simply rank corrosion-resistant

alloys based on its corrosion performance in concentrated HCl and H₂SO₄ acid but to demonstrate a mechanism of the role of alloying elements in an alloy to its performance in concentrated acidic solutions.

Another part of the study focuses on the localized corrosion behavior of the Ni–Cr–Mo (W) alloys in chloride-rich environment. It is widely known that in Cr-enriched alloys, irrespective of the base metal, chromium forms the primary Cr₂O₃ passive film which is dominantly responsible for passivation while Mo (and W) is known to inhibit localized corrosion by oxide reformation within initiated pits, thereby retarding their growth [5, 11–22]. Despite the excellent general corrosion resistance of Ni–Cr–Mo (W) alloys in a wide range of acidic solutions, these alloys can experience localized corrosion (particularly crevice corrosion) in oxidizing concentrated saline solutions at temperatures below 100 °C [7].

There are multiple articles published in the last decade on the crevice corrosion study of Ni–Cr–Mo (W) alloys from academic research groups; however, almost all of these studies were performed in sodium chloride solution (NaCl) and utilized conservative electrochemical techniques to force the material to corrode [7, 14–22]. Although the information generated on this topic from the academic laboratories is very useful in understanding the mechanism of the crevice corrosion, the data may or may not be of much use to the industrial researchers. Therefore, the present study also focuses on trying to correlate the localized corrosion data obtained using ASTM G-48 test methodology [23], a widely used technique by industrial researchers to determine the susceptibility of Fe-based alloys and Ni-based alloys to localized corrosion, to the scientific data generated in the academic laboratories.

While the actual choice of an alloy for an application is made on the basis of field experience, this research article will enable an initial selection of a set of alloys to be used for further field testing in a given environment.

2 Experimental

2.1 Corrosion Test

Corrosion tests were conducted on HASTELLOY[®] G-35[®], C-2000[®], C-22[®], C-22HS[®], C-276, HYBRID-BC1[®], B-3[®] alloys, HAYNES[®] 718 and HAYNES[®] 625 alloys,¹ alloy 59 and alloy 686. The nominal compositions of the studied alloys are shown in Table 1.

¹Par¹ HASTELLOY[®], HAYNES[®], G-35[®], C-2000[®], C-22[®], C-22HS[®], HYBRID-BC1[®] and B-3[®] are registered trademarks of Haynes International, Inc.

Table 1 Weight percent of major alloying elements in Ni–Cr–Mo (W) alloys

Alloys (UNS Number)	Cr	Mo	W	Cu	Ni
G-35 (N06035)	33	8			Bal.
C-2000 (N06200)	23	16		1.6	Bal.
Alloy 59 (N06059)	23	16			Bal.
C-22 (N06022)	22	13	3		Bal.
C-22HS (N07022)	21	17			Bal.
Alloy 686 (N06686)	21	16	4		Bal.
C-276 (N10276)	16	16	4		Bal.
HYBRID-BC1 (N10362)	15	22			Bal.
B-3 (N10675)	1.5	28.5			Bal.
Alloy 718 (N07718)	18	3			Bal.
Alloy 625 (N06625)	21	9			Bal.

Corrosion tests of the wrought alloys were carried out under laboratory conditions using glass flask/condenser systems and reagent grade chemicals. The coupon dimensions were 25 mm × 25 mm × 3 mm. The surfaces of these coupons were ground using 120- to 600-grit papers and then degreased with acetone, prior to weighing followed by testing of the coupons. A test duration of 96 h was selected, with interruptions every 24 h to weigh the coupons. The solution used was concentrated HCl acid and H₂SO₄ acid of various concentrations and temperatures. Corrosion studies were also performed in HCl solutions to which various amounts of oxidizing impurity had been added.

Immersion corrosion tests were also conducted to determine the critical pitting temperature (CPT) and critical crevice temperature (CCT) of the studied alloys using the guidelines in ASTM G-48C and G-48D [23]. The ASTM G-48 test solution was acidified ferric chloride (6% FeCl₃ + 1% HCl), and the immersion time was 72 h.

2.2 Electrochemical Test

For electrochemical measurements, specimens with a total surface area of ~14 cm² were cut from the plate materials. A small tapped hole was machined in the top of the specimen to enable contact, via a cylindrical rod, to external circuitry. This rod was sheathed in glass and sealed with a polytetrafluoroethylene (PTFE) gasket to prevent contact with the electrolyte. The specimen was then polished with a series of wet silicon carbide papers up to 600 grit, rinsed with deionized water and acetone, and then air-dried prior to an experiment. A platinum (Pt) foil and a saturated calomel electrode (SCE) were used as the counter and reference electrode, respectively.

The electrochemical tests were performed in deaerated HCl and H₂SO₄ acid of various concentrations. The open-circuit potential (OCP) was recorded for 1 h to allow a near steady-state value to be approached. Subsequently, linear polarization resistance (LPR) measurements were conducted as per ASTM G-59 [23], from –20 to +20 mV of the E_{corr} . Upon completion of LPR experiment, OCP was recorded for 20 min to allow a near steady-state value followed by potentiodynamic polarization (PP) tests. Potentiodynamic polarization test was performed from –250 mV below E_{corr} to +1100 mV above at a scan rate of 0.167 mV/s in the forward direction. To study the effects of impurities in HCl on the corrosion behavior, electrochemical experiments (OCP, LPR and PP) were conducted in 20% HCl containing various concentrations of Fe³⁺ ions.

2.3 Characterization Techniques

The specimens were analyzed via optical microscopy, scanning electron microscopy (SEM) and X-ray photoelectron spectroscopy (XPS). Optical microscopy was performed with a Leica DMI5000 M inverted research microscope and DFC425 digital microscope camera. SEM was conducted with a ZEISS SUPRA 40 field emission scanning electron microscope (FESEM).

Electrodes anodically oxidized for surface analyses were rinsed gently with DI water and air-dried prior to characterization. XPS analyses were completed with a Kratos Axis Ultra XPS at Surface Science Western (SSW, Canada) employing monochromatic Al K_α (1486.8 eV) radiation. The binding energy was calibrated to give a Au 4f_{7/2} line position at 83.95 eV. XPS spectra were corrected for charging by taking the C 1 s spectrum for adventitious carbon to be at a binding energy of 284.8 eV. Survey spectra were recorded on specimens followed by high-resolution XPS spectra for Ni 2p, Cr 2p, Mo 3d, W 4f, C 1 s and O 1 s spectral regions.

3 Results and Discussion

Figure 1 shows a typical microstructure of mill-annealed C-2000, G-35, HYBRID-BC1 and B-3 alloys. Based on the alloying composition, C-2000 and G-35 alloys contain high amount of Cr, and HYBRID-BC1 and B-3 alloys have a high amount of Mo (Table 1). The microstructures of HYBRID-BC1 (Fig. 1c) and B-3 (Fig. 1d) alloys show a small volume fraction of second phase, presumably a Mo-enriched phase, distributed over the grains. The presence of small volume fraction of second phase in the mill-annealed microstructure can be attributed to high amount of Mo, 22% in HYBRID-BC1 and 28.5% in B-3, added as an

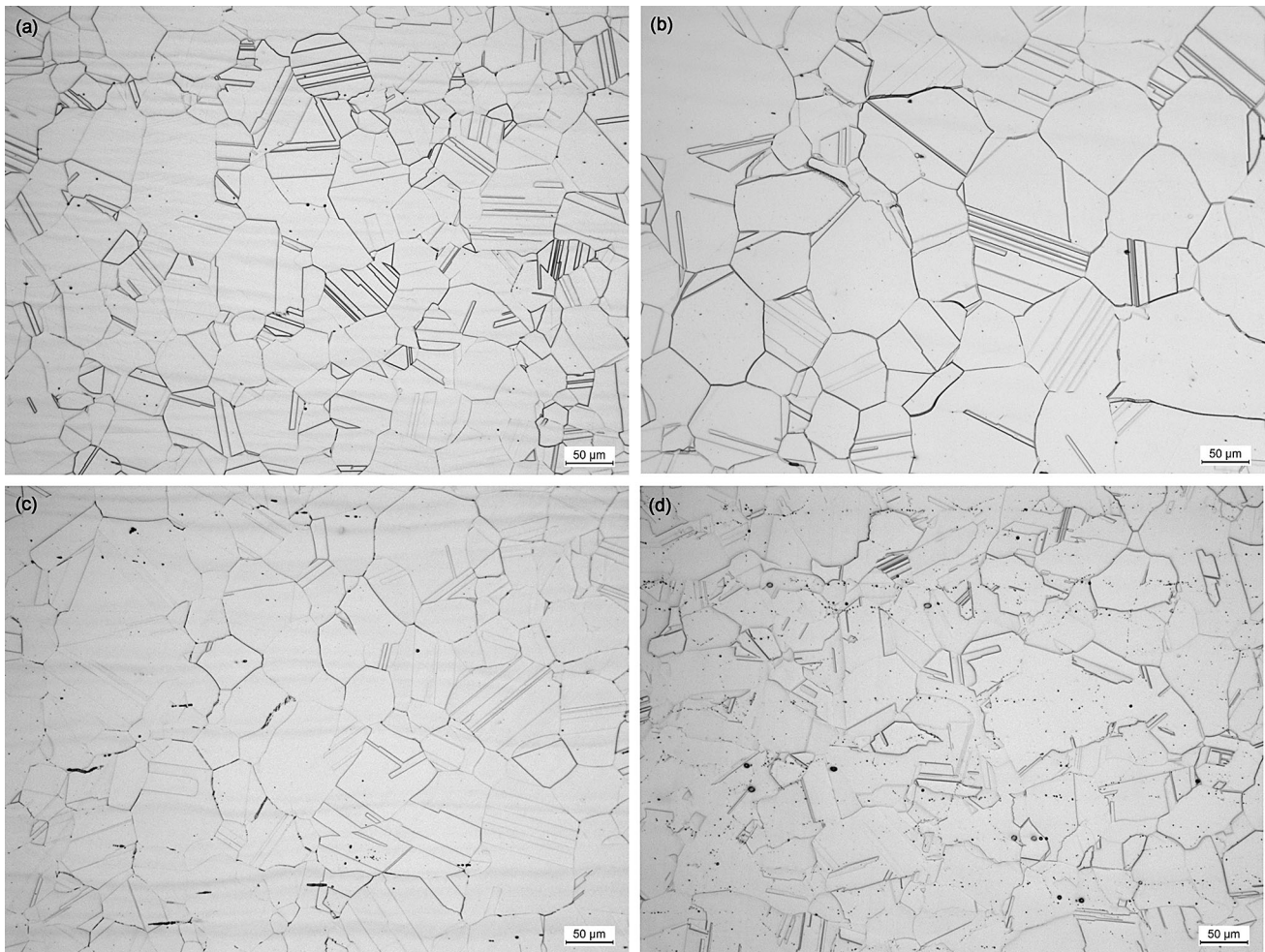


Fig. 1 Microstructures of mill-annealed **a** C-2000, **b** G-35, **c** HYBRID-BC1, **d** B-3 alloys

alloying element. It should be noted that the volume fraction of second-phase particle is low, small in size and distributed over the grains and not segregated on the grain boundaries. Therefore, these high Mo-containing alloys (B-3, HYBRID-BC1) do not experience a deterioration in its corrosion resistance property in aggressive environments despite the presence of second-phase particle.

3.1 Materials Performance in HCl Acid (with and without oxidants)

Figures 2, 3, 4, 5 and 6 show the iso-corrosion curve generated in reagent grade HCl acid (up to 37 wt%) for B-3, HYBRID-BC1, C-276, C-2000 and C-22 alloys, respectively. Iso-corrosion diagram of an alloy is generated from the weight loss data after immersion testing in reagent grade solutions and in a laboratory environment which may or may not replicate the field conditions. However, it is a very useful diagram to understand the uniform corrosion performance of an alloy in an aggressive solution. In the present study, iso-corrosion lines of 0.1 mm/y (4 mpy),

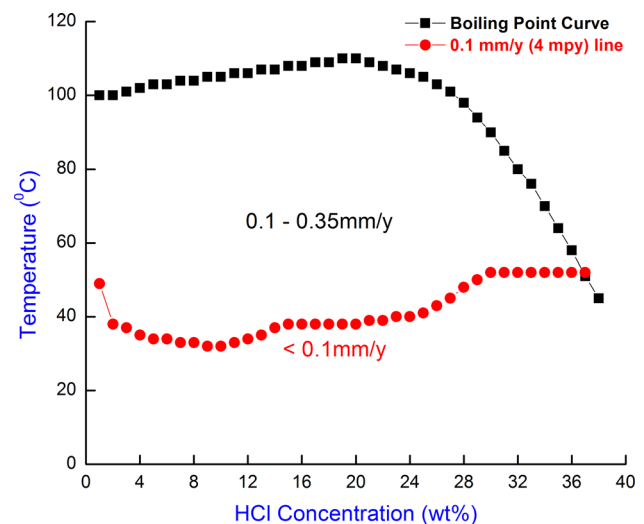


Fig. 2 Iso-corrosion diagram of B-3 alloy in HCl solution

0.5 mm/y (20 mpy), 1.3 mm/y (50 mpy) and 2.5 mm/y (100 mpy) were constructed for various corrosion-resistant alloys in the reagent grade HCl acid below its boiling point.

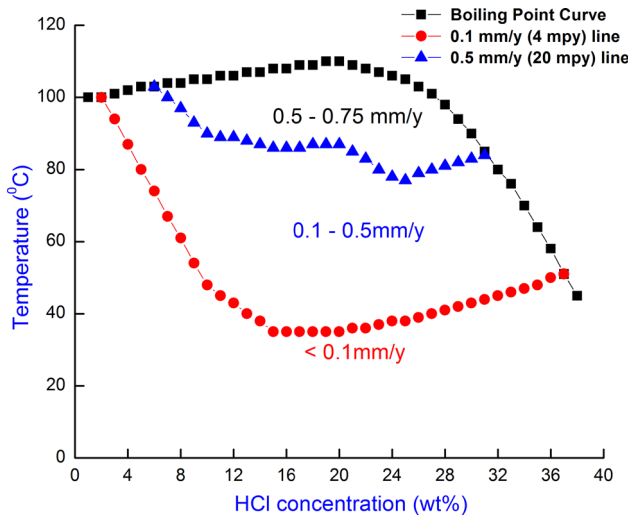


Fig. 3 Iso-corrosion diagram of HYBRID-BC1 alloy in HCl solution

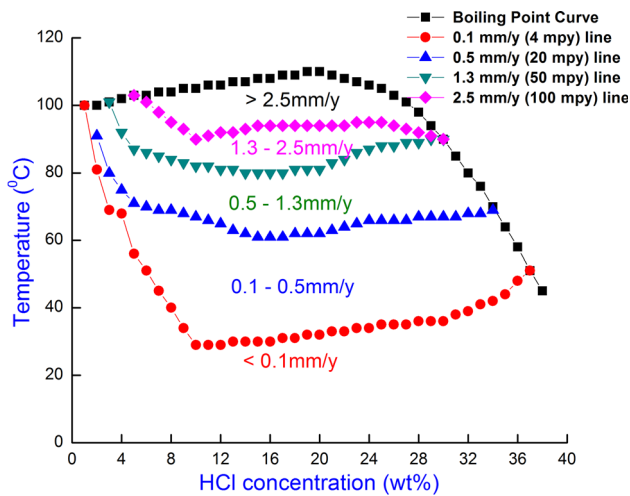


Fig. 4 Iso-corrosion diagram of C-276 alloy in HCl solution

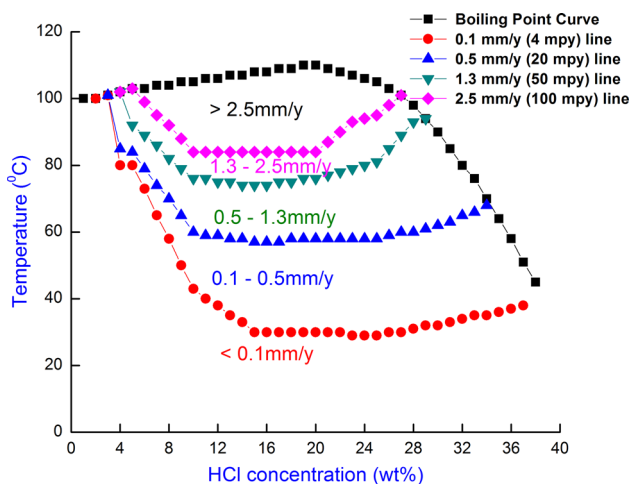


Fig. 5 Iso-corrosion diagram of C-2000 alloy in HCl solution

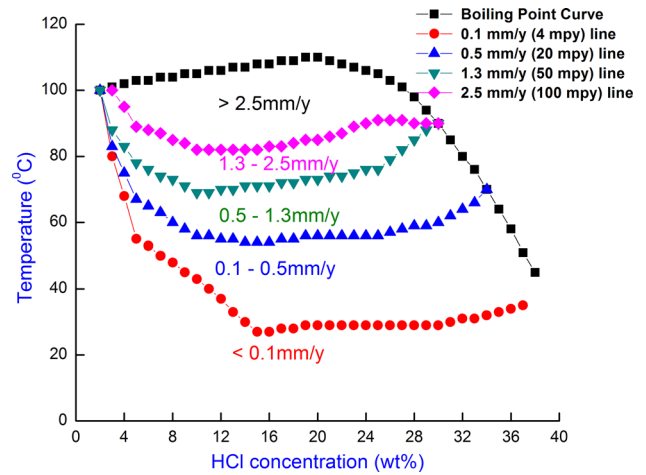


Fig. 6 Iso-corrosion diagram of C-22 alloy in HCl solution

The corrosion rate of B-3 alloy in reagent grade HCl acid is less than 0.1 mm/y below the red line and 0.10–0.35 mm/y in between red line and the boiling point curve for HCl, as shown in Fig. 2. It can be concluded from the iso-corrosion graph that the maximum corrosion rate of B-3 alloy in reagent grade HCl acid for concentration up to 37 wt% and temperature up to its boiling point is less than 0.35 mm/y. For HYBRID-BC1 alloy (Fig. 3), iso-corrosion lines of 0.1 and 0.5 mm/y were drawn and the maximum corrosion rate calculated in HCl acid below its boiling point is approximately 0.75 mm/y. The corrosion rates obtained for C-276, C-2000 and C-22 alloys (Figs. 4, 5, 6) are much higher than those for B-3 and HYBRID-BC1 alloys in similar conditions. The iso-corrosion lines for various alloys assist the industrial researchers in choosing the right set of alloys for further investigation.

Figures 7 and 8 compare the 0.1 mm/y (4 mpy) and 0.5 mm/y (20 mpy) iso-corrosion line for various alloys, and the graph shows that the uniform corrosion resistance

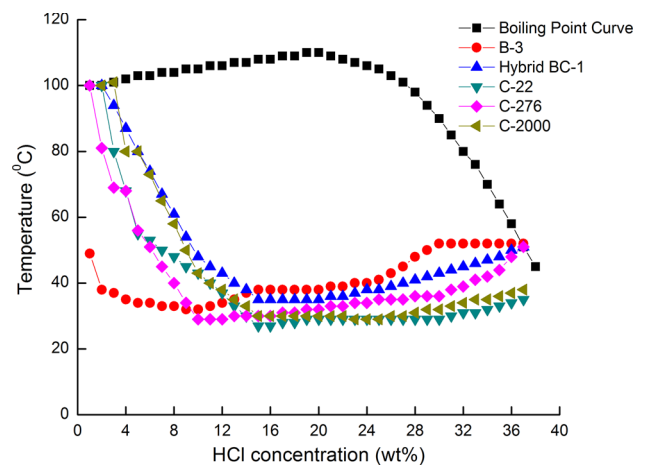


Fig. 7 Temperature calculated to induce corrosion rate of 0.1 mm/y (4 mpy) in reagent grade HCl solution

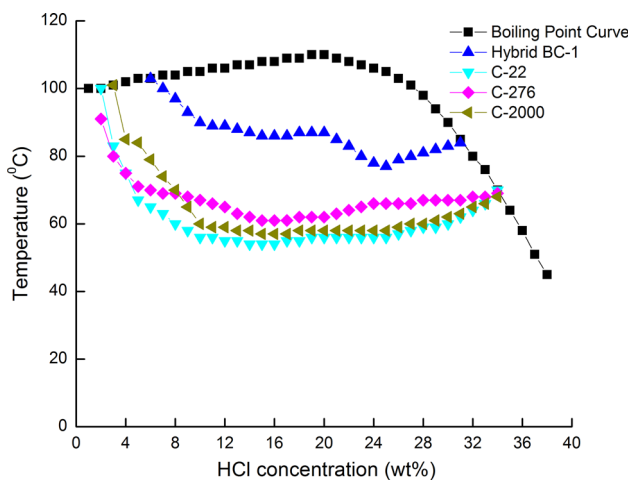


Fig. 8 Temperature calculated to induce corrosion rate of 0.5 mm/y (20 mpy) in reagent grade HCl solution

of alloys in HCl acid is a strong function of the amount of Mo (or Mo + 0.5 W) in an alloy, i.e., higher the amount of Mo (or Mo + 0.5 W), higher is its uniform corrosion resistance. It is a known fact that corrosion resistance mechanism of W is similar to Mo [4, 6, 7]; however, for a similar contribution to the corrosion resistance performance, the amount of W (in wt%) in an alloy needs to be almost double of that of Mo [4, 7]. This is also a reason that the “effective Mo amount” in an alloy containing both Mo and W is equivalent to %Mo + 0.5%W. The corrosion rate of B-3 alloy did not exceed 0.5 mm/y at the studied concentration and temperature of HCl acid, so a 0.5 mm/y iso-corrosion line of B-3 alloy cannot be constructed.

Based on the corrosion resistance performance in reagent grade HCl at the studied concentrations and temperature, the alloys can be ranked (high to low) as $B-3 > HYBRID-BC1 > C-276 > C-2000 > C-22$. (1)

The ranking follows the same trend as the amount of Mo (or Mo + 0.5 W) in the respective alloys, which decreases in the same sequence from B-3 (28.5 wt% Mo), HYBRID-BC1 (22 wt% Mo), C-276 (18 wt%; 16Mo + 4 W is equivalent to 18% Mo), C-2000 (16 wt% Mo) and the lowest in C-22 (14.5 wt%; 13Mo + 3 W is equivalent to 14.5% Mo) alloy.

Interestingly, the corrosion rate of B-3 alloy reaches 0.1 mm/y in lower concentrations of HCl acid at a much lower temperature compared to other studied alloys (Fig. 7) which deviates from the notion that higher Mo results in a high corrosion resistance in any concentration of HCl acid. It is anticipated that in a less aggressive HCl acid, an optimum amount of Cr is also needed in addition to higher amount of Mo to provide good corrosion resistance (B-3 contains only 1.5 wt% Cr), though more research work is needed to understand the role of alloying

elements in an alloy to its corrosion performance in less aggressive HCl solution.

In order to give a scientific meaning to the weight loss data, electrochemical experiments were conducted on corrosion-resistant alloys in various concentrations of HCl acid. Figure 9 shows the potentiodynamic polarization (PP) graphs for C-22 alloy in 5–30% HCl at room temperature. The PP graph shows that in a less aggressive solution (5 wt%), the passive current density is low and the passive range is high due to formation of a highly protective chromium oxide (Cr₂O₃) passive film. When the solution is relatively aggressive (20 wt%), the material experiences an active–passive transition, lower passive current density and a relatively smaller passive range which can be attributed to slightly defective passive film. A further increase in the solution concentration to 30 wt% results in a sudden increase in the current at a relatively lower anodic potential. Since the current reaches the current limit of the potentiostat when anodically scanned at 30 wt%, it is difficult to conclude that if the material will form any passive film at higher anodic potential or not. However, undoubtedly, an increase in the solution concentration deteriorates the protectiveness of the passive film.

Generally, the industrial acids are frequently contaminated with oxidizing impurities such as ferric salts and other cationic species added by corrosion or unremoved during processing. For example, ferric ions are often found in process streams and cleaning applications, where a strong reducing acid such as HCl is required. Therefore, in the present study, corrosion experiments were also conducted in HCl acid containing various concentrations of oxidants (ferric ion), as shown in Table 2 and Fig. 10. The data reported in Table 2 and Fig. 10 show the corrosion

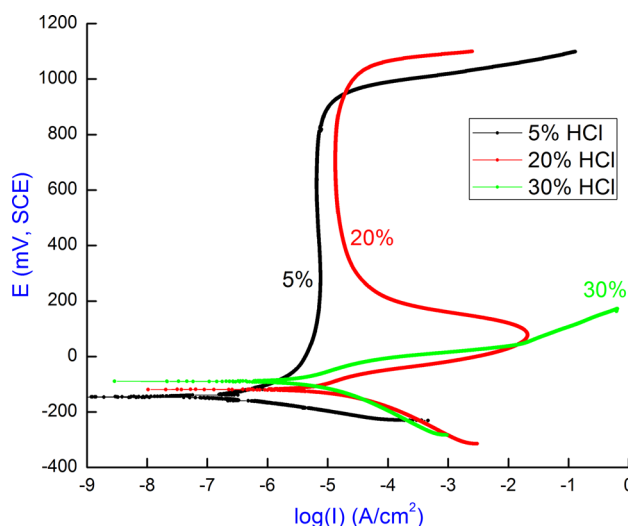
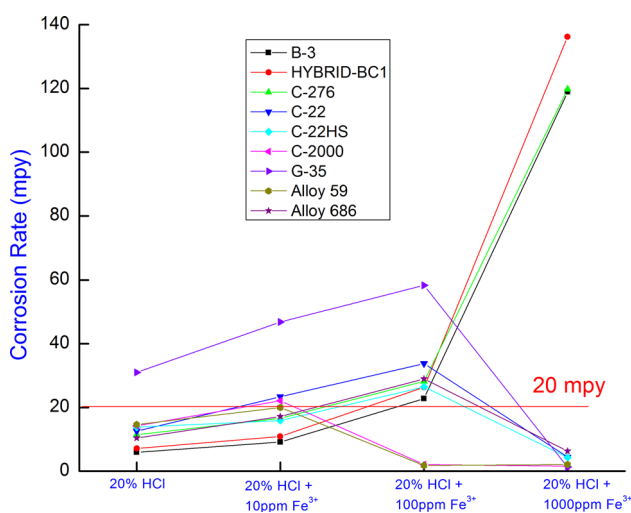


Fig. 9 Potentiodynamic polarization graphs of C-22 alloy in various concentrations of HCl acid at room temperature

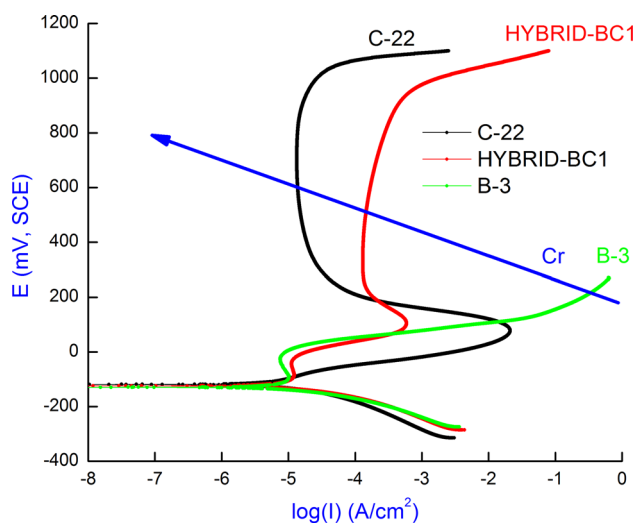
Table 2 Corrosion rate of corrosion-resistant alloys in HCl solution and HCl solution containing oxidants

Alloy	20% HCl (mpy)		20% HCl + 10 ppm Fe ³⁺ (mpy)		20% HCl + 100 ppm Fe ³⁺ (mpy)		20% HCl + 1000 ppm Fe ³⁺ (mpy)	
	23 °C	52 °C	23 °C	52 °C	23 °C	52 °C	23 °C	52 °C
B-3	1.4	5.9	2.0	9.1	4.9	22.8	44.8	118.9
HYBRID-BC1	1.6	7.1	1.8	10.9	5.8	26.3	7.6	136.2
C-276	1.6	11.4	1.8	16.6	6.5	28.2	5.0	119.7
C-22	2.0	12.6	2.4	23.3	0.4	33.8	0.3	4.4
C-22HS	2.0	13.8	1.9	15.9	0.3	26.5	0.6	4.3
C-2000	2.0	14.2	2.3	22.1	0.4	2.1	0.3	1.6
G-35	6.1	31.0	7.8	46.8	0.2	58.3	0.1	1.3
Alloy 59	2.1	14.6	2.1	20.0	0.4	1.8	0.1	2.1
Alloy 686	2.2	10.4	2.0	17.1	6.6	29.0	0.5	6.3

**Fig. 10** Effect of oxidants on the corrosion performance of CRA's (temp.: 52 °C)

rate of commercial Ni–Cr–Mo (W) alloys in HCl acid (with and without oxidants).

As concluded above, in pure HCl acid, the uniform corrosion rate is a strong function of the amount of Mo (or Mo + 0.5 W); therefore, G-35 alloy (8 wt% Mo) has the highest corrosion rate and B-3 alloy (28.5 wt% Mo) experienced the lowest uniform corrosion rate. But in the presence of 1000 ppm ferric ions (a strong oxidizing ion), G-35 alloy containing the highest Cr (33 wt%) has a significantly lower corrosion rate than alloys containing lower amount of Cr, like B-3, HYBRID-BC1 and C-276 alloys (Table 1). Although the weight loss data provide a good overview of the materials performance in HCl acid (with and without oxidants), it fails to demonstrate an exact corrosion mechanism. Therefore, electrochemical experiments were performed on various corrosion-resistant alloys in HCl acid and few of them are reported in the present study (Fig. 11).

**Fig. 11** Potentiodynamic polarization graphs of corrosion-resistant alloys in 20% HCl acid at room temperature

The potentiodynamic polarization graphs (Fig. 11) recorded in 20% HCl clearly showed a strong relationship between alloy Cr content and the passivation current density with a high amount of Cr resulting in a low passivation current density (i_p). A low i_p can be attributed to the presence of a protective and less defective passive film. The potentiodynamic polarization study showed that no passive film was formed on B-3 alloy. Since Fe³⁺ is a strong oxidant, the absence of a passive film (Fig. 11) resulted in a high corrosion rate on B-3 alloy in 20% HCl + 1000 ppm Fe³⁺ (Table 2). The corrosion data obtained from weight loss technique show that in 20% HCl + 1000 ppm Fe³⁺ at room temperature, the corrosion rate of B-3 alloy is the highest (44.8 mpy) among the studied alloys. In a similar environment, the corrosion rate of HYBRID-BC1 alloy (containing 15 wt% Cr) is higher than of C-22 alloy (22 wt% Cr) (Table 2). Thus, it can be concluded from the weight loss

data and electrochemical results that in the presence of high amount of oxidizing impurity, alloys containing high amount of Cr are better choice of materials. Lloyd et al. [5] studied the passive film properties of a number of Ni–Cr–Mo (W) alloys (C-4, C-276, C-22, C-2000 and Alloy 625) at different potentials and temperatures in acidic solutions by using various electrochemical and surface characterization techniques, and it was suggested that high Cr (>20 wt%)-containing alloys (like C-22, C-2000) demonstrated better passive film properties than low Cr-containing alloys (like C-4, C-276).

Potentiodynamic curves were also obtained for C-22 and HYBRID-BC1 alloys in 20%HCl acid + *x* ppm ferric ion (*x*: 0, 10 and 1000) (Fig. 12). Although the PP curve in 20%HCl and 20%HCl + 10 ppm Fe³⁺ looks nearly similar for both alloys, however, for 20%HCl + 1000 ppm Fe³⁺ there is an increase in the open-circuit potential (OCP) by approximately 550 mV. An increase in hundreds of mV in OCP, for both C-22 and HYBRID-BC1 alloys, is a result of strong oxidizing nature of the ferric ion. Also, the shape of potentiodynamic graph in the presence of high concentration of Fe³⁺ is different for C-22 compared to HYBRID-BC1 alloy (Fig. 12).

To demonstrate the role of oxidants (like ferric ion, cupric ion and aerated environment) in more detail, a schematic illustrating the oxidants (Fe³⁺) effect on the corrosion performance of Ni-based alloys is shown in Fig. 13. The figure includes two polarization curves, one for a low Mo (Mo + W)-high Cr alloy (black curve) and another for a high Mo (Mo + W)-low Cr alloy (red curve). A sufficient concentration of added Fe³⁺ (leading to the cathodic current potential relationship indicated by the blue line) will lead to an OCP in the passive region as indicated by the intersection of the blue line with the two polarization curves. Under these conditions, the passive current

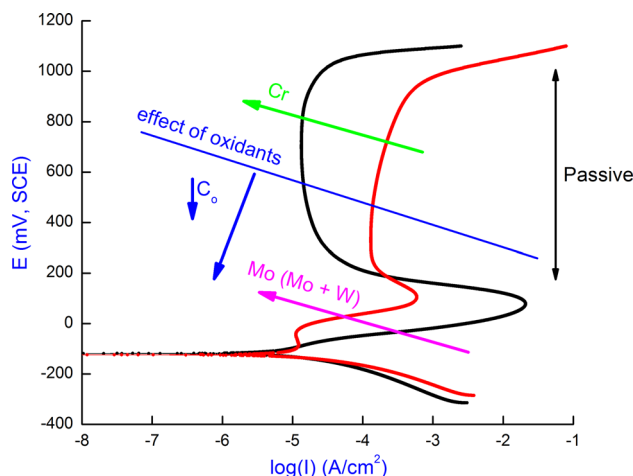


Fig. 13 Schematic of effect of oxidants on the corrosion performance of Ni–Cr–Mo (W) alloys. Graph also shows the active and passive regions for the black curve

(and hence the corrosion rate) would be lower on the high Cr alloy (indicated by the green arrow). However, if the Fe³⁺ concentration was less than the critical current density (the peak current during the active to passive transition), the blue line would eventually shift to lower potentials and into the active region as indicated by the blue arrows (with *C*_o indicating the decrease in oxidant concentration). Under these conditions, the corrosion rate would be expected to decrease as the Mo (Mo + W) content of the alloy increased which is consistent with our observations. The presence of ferric ions (or oxidizing ions in general) in HCl solution, or any aqueous solution, simply influences the overall cathodic reaction due to the reduction of ferric ions to a lower oxidation state. Thus, among Ni–Cr–Mo (W) alloys, an alloy having higher amount of Cr will demonstrate a better corrosion resistance in HCl solution containing high amount of ferric ions (Table 2).

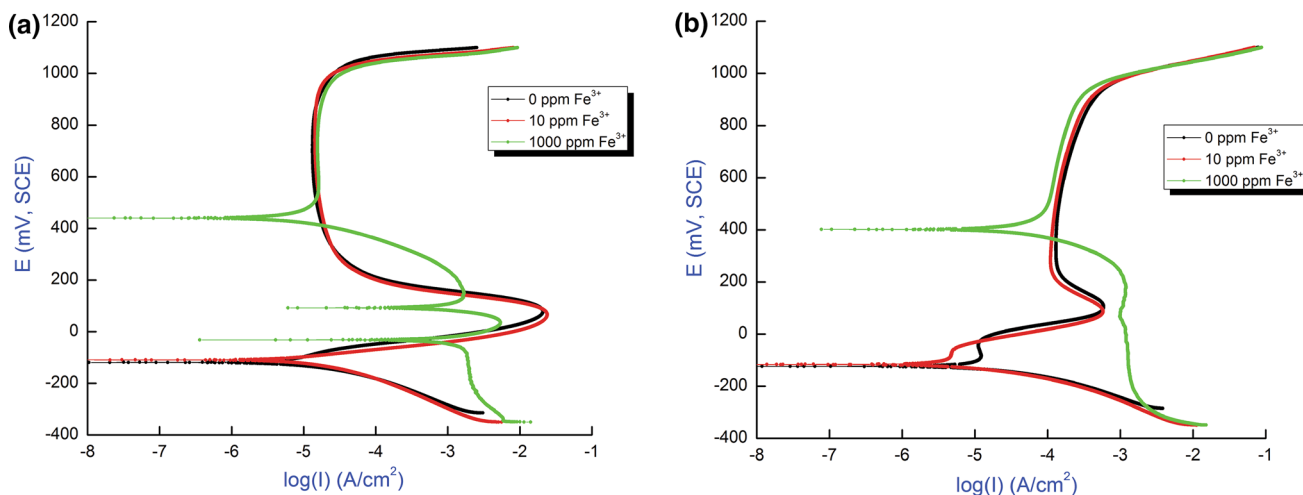


Fig. 12 Potentiodynamic graphs in 20% (wt%) HCl, with and without impurity, at an ambient temperature for **a** C-22; **b** HYBRID-BC1

Another interesting observation in the potentiodynamic curves in HCl solution is the anodic current behavior in the active region (i.e., between the corrosion potential and the active–passive transition) for alloys enriched in Mo (or Mo + W) (Fig. 13). The current arrest at potentials lower than the active to passive transition indicates a distinct suppression of active dissolution as the Mo (Mo + W) content is increased.

XPS technique was used to analyze the composition of the oxide films present at free corroding potential (hold time as 5 h at OCP) or potentiostatic polarization in the passive region (500 mV vs SCE; hold time as 5 h) in 20% HCl. For comparison, the composition of the native oxide (formed by air exposure) was also determined. Figure 14 shows the atomic concentration (expressed as at.% of cation content) obtained from XPS survey spectra. In the air-formed film, the Cr is enriched as expected, but the film is dominated by the Ni content. In the passive region, the alloy is enriched in Cr and depleted in Ni. At OCP, the surface of HYBRID-BC1 alloy is strongly depleted in Ni but enriched in Mo not Cr (Fig. 14). The preliminary XPS survey spectra data on HYBRID-BC1 alloy suggest that with an increase in Mo (or Mo + W) content the corrosion rate decreases in a strong reducing acid (like HCl acid), whereas with an increase in Cr content an alloy will demonstrate a high corrosion resistance performance in an oxidizing condition (like HCl + 1000 ppm Fe³⁺). The results are in consensus with the weight loss (Table 2; Fig. 10) and the electrochemical data (Figs. 11, 12, 13).

3.2 Materials Performance in H₂SO₄ Acid

Figures 15 and 16 show the 0.1 and 0.5 mm/y iso-corrosion line obtained for various corrosion-resistant alloys in

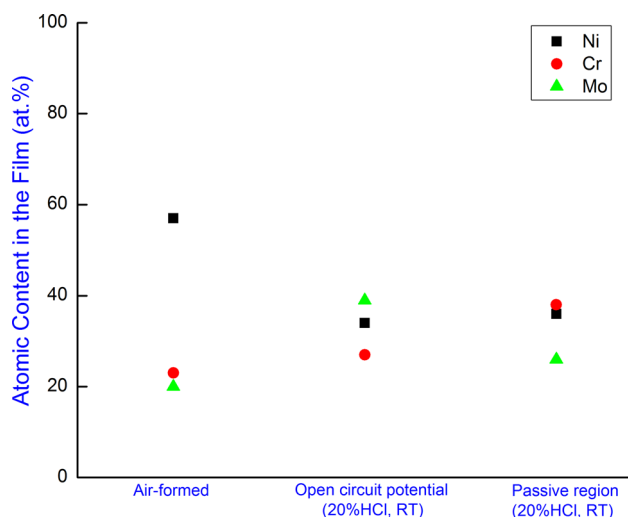


Fig. 14 Atomic concentration of major alloying elements obtained from XPS survey spectra for HYBRID-BC1 alloy

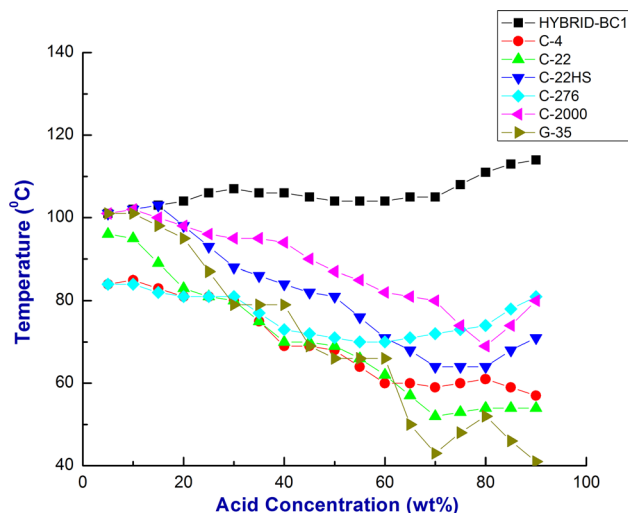


Fig. 15 Temperature calculated to induce corrosion rate of 0.1 mm/y (4 mpy) in reagent grade H₂SO₄ acid

reagent grade H₂SO₄ acid up to 90 wt%. Similar to HCl acid, the corrosion resistance of alloys containing high Mo (Mo + 0.5 W) demonstrates a high corrosion resistance in reagent grade H₂SO₄ acid. Among the studied alloys, HYBRID-BC1 (22 wt% Mo) has the highest uniform corrosion resistance and G-35 (8 wt% Mo) alloy the lowest.

Although not reported in the present study, B-3 alloy which contains even higher Mo than HYBRID-BC1 can be considered as the most corrosion-resistant alloy in reagent grade H₂SO₄ alloy. However, a very low amount of Cr in B-3 alloy results in a significantly high corrosion rate in the presence of oxidizing impurities, irrespective of the base medium as HCl (Table 2) or H₂SO₄ or any other solution. Therefore, extra caution must be taken in considering B-3 alloy if there is a possibility that the material can be exposed to a solution containing oxidants.

Based on the Mo (Mo + 0.5 W) content (Table 1), the corrosion resistance performance in reagent grade H₂SO₄ should be ranked (high to low), among the studied alloys, as

$$\text{HYBRID-BC1} > \text{C-276} > \text{C-22HS} > \text{C-2000} \sim \text{C-4} > \text{C-22} > \text{G-35}. \quad (2)$$

However, the actual ranking from the weight loss data (Figs. 15 and 16) shows a slight deviation, i.e.,

$$\text{HYBRID-BC1} > \text{C-2000} > \text{C-276} > \text{C-22HS} > \text{C-4} > \text{C-22} > \text{G-35}. \quad (3)$$

The corrosion data show that C-2000 alloy has a much higher corrosion resistance in H₂SO₄ acid than expected. In a recent study, Mishra et al. [24] investigated the oxide film formation on C-2000 alloy at different pH using angle-resolved x-ray photoelectron spectroscopy (AR-XPS) and

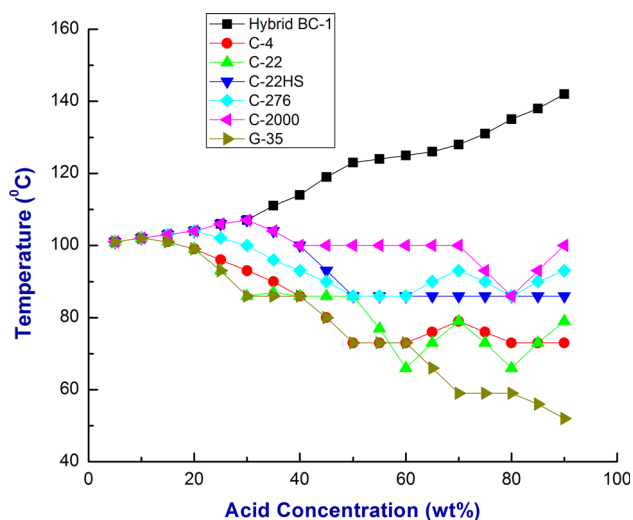


Fig. 16 Temperature calculated to induce corrosion rate of 0.5 mm/y (20 mpy) in reagent grade H_2SO_4 acid

time-of-flight secondary ion mass spectroscopy (TOF-SIMS). It was observed from the surface-sensitive techniques that the copper segregated to the oxide/solution interface during anodic film growth and this process was enhanced as the pH decreased. Sridhar [25] claimed a beneficial role for Cu addition in Ni-22Cr-6Mo-25Fe in various concentrations of sulfuric acid. The corrosion data showed that addition of even a small amount of Cu (~ 2 wt%) significantly reduced the corrosion rate in high concentrations of sulfuric acid. Crook [26, 27], an inventor of the Cu-containing C-2000 alloy, investigated the corrosion performance of this alloy in a wide range of corrosive media and clearly demonstrated a higher uniform corrosion resistance of C-2000 alloy compared to other corrosion-resistant Ni–Cr–Mo alloys in H_2SO_4 acid. Although more characterization study is needed to understand the role of Cu in C-2000 alloy, the present and previous studies [24–27] clearly support the notion that the presence of Cu (1.6 wt%) in C-2000 alloy (Table 1) enhances the uniform corrosion resistance performance in reagent grade H_2SO_4 acid. Except C-2000 alloy, the ranking of various Ni–Cr–Mo (W) alloys based on its corrosion resistance performance in HCl and H_2SO_4 behaves similarly, i.e., higher the Mo (or Mo + 0.5 W) content, the higher will be its uniform corrosion resistance.

To understand the solution chemistry of H_2SO_4 , Sridhar [28] obtained the redox potential of platinized platinum at various concentrations of reagent grade H_2SO_4 acid. It was concluded that for concentration of H_2SO_4 below ~ 70 wt%, the solution act as a strong reducing acid. However, above ~ 70 wt%, the redox potential exhibits a steep increase with acid concentration. Hibner and Shoemaker [29] proposed that “dilute H_2SO_4 acid is very reducing in nature but at greater concentrations, it begins to take on an

oxidizing character. Thus, dilute and intermediate strengths of the acid can be contained by materials resistant to reducing conditions while stronger concentrations require materials resistant to oxidizing media.” However, contrary to the previous studies, the iso-corrosion diagrams (Figs. 15, 16) in the present study did not suggest a shift in the reducing nature of the H_2SO_4 to oxidizing at higher concentrations.

Potentiodynamic polarization experiments were conducted on C-2000 alloy for different concentrations of H_2SO_4 acid (Fig. 17) at room temperature. The result shows that there is a slight increase in the OCP value of C-2000 alloy at high concentration (like 80 wt%) compared to low concentration (like 30 wt%), but the passive region, active–passive current density and the passivation current density are almost similar despite an increase in the concentration. Furthermore, the weight loss data (Figs. 15, 16) also demonstrate that an alloy containing high Mo (like HYBRID-BC1) shows a high corrosion resistance in various concentrations and temperatures of the H_2SO_4 (up to 90 wt%).

Figure 18 shows an iso-corrosion curve for HYBRID-BC1 alloy up to 96 wt% H_2SO_4 acid. It should be noted that the maximum concentration of reagent grade H_2SO_4 is 96 wt% and above that it is a commercial grade. The iso-corrosion curve demonstrates a slightly higher corrosion rate for the concentration of H_2SO_4 above 90 wt%, as seen from a slight dip in the 0.1 mm/y iso-corrosion line (blue line) above 90 wt%, but no deviation in 0.5 mm/y iso-corrosion line (red line) can be seen for concentration above 90 wt%. The iso-corrosion curve of HYBRID-BC1, for concentration of H_2SO_4 acid to as high as 96 wt% (Fig. 18), further validates that even at very high

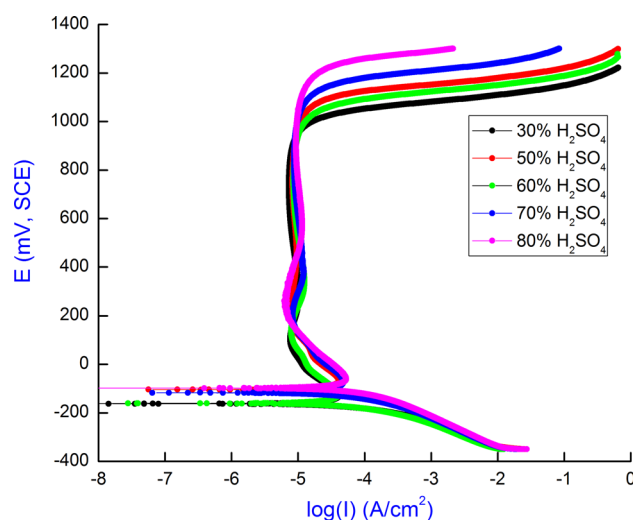


Fig. 17 Potentiodynamic polarization graphs of C-2000 alloy in various concentrations of reagent grade H_2SO_4 acid at room temperature

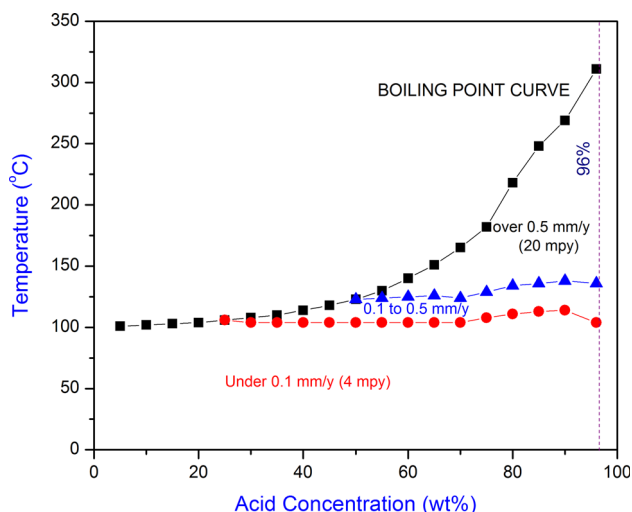


Fig. 18 Iso-corrosion diagram of HYBRID-BC1 alloy in H_2SO_4 acid

concentrations, an alloy containing high Mo will exhibit a high uniform corrosion resistance performance. Thus, the corrosion data in the present study refute the earlier notion that “higher concentration of H_2SO_4 acid requires materials resistant to oxidizing media” [29].

Potentiodynamic polarization curves for B-3 alloy were obtained for various concentrations of reagent grade H_2SO_4 acid at room temperature, as shown in Fig. 19. The graphs clearly show that with an increase in the concentration of H_2SO_4 acid, there is an increase in the pseudo-protective range (marked as vertical arrows in Fig. 19). B-3 alloy contains almost no Cr, so an increase in the pseudo-protection range for B-3 alloy is associated with the Mo (and its oxides). Although it is not feasible to conclude from electrochemical data, without a rigorous surface analysis, it is anticipated that with an increase in the concentration of H_2SO_4 acid the oxides

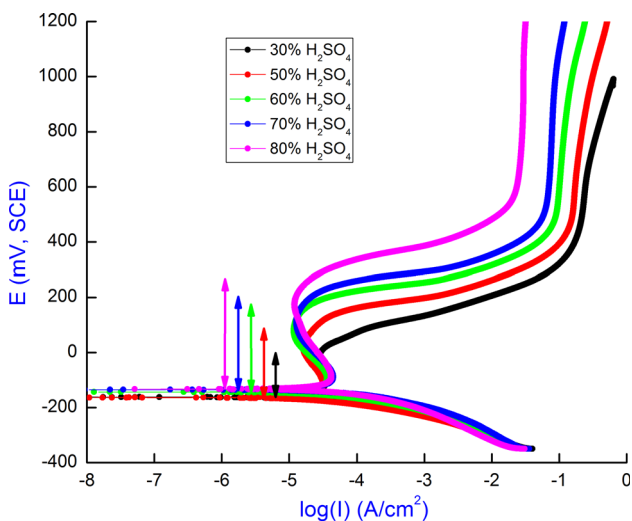


Fig. 19 Potentiodynamic polarization graphs of B-3 in various concentrations of reagent grade H_2SO_4 acid at room temperature

of Mo becomes more protective which is evident from an increase in the pseudo-protective range (Fig. 19).

An attempt was made in the present study to investigate the surface oxide film formed on C-2000 alloy after immersion in 80 wt% H_2SO_4 at 107 °C for 4 days through optical microscope and SEM/EDX technique (Fig. 20). As expected, EDX technique (spot analysis or mapping) was unable to determine the composition of surface film as the thickness of the oxide film is in nanometers which is beyond the detection limit of SEM/EDX technique. Future studies are planned to observe the oxide film formation on corrosion-resistant Ni–Cr–Mo alloys, after immersion in concentrated H_2SO_4 acid at an optimum temperature, using XPS and Auger electron spectroscopy (AES) techniques. As materials perform in nearly a similar manner in both HCl and H_2SO_4 acid, there is a good possibility that the top layer of the oxide film when exposed to concentrated H_2SO_4 acid will show an enrichment of Mo (or Mo + W).

3.3 Localized Corrosion Performance of Corrosion-Resistant Alloys

Metals or alloys which form a passive film are widely used in aggressive environments as passivity reduces the dissolution rate by orders of magnitude. Naturally occurring passive films exhibit good corrosion resistance, but breakdown of the film can lead to a susceptibility to localized corrosion. Localized corrosion occurs at a rapid rate, is difficult to detect during service and can cause unexpected catastrophic failure [30]. From the localized corrosion perspective, in Ni–Cr–Mo (W) alloys, Cr has the primary influence on maintaining passivity [5], and Mo and W help to control localized corrosion propagation and aid in repassivation [6–8, 15, 20, 22]. Thus, optimizing the concentrations of Cr, Mo and W is a key feature in developing Ni–Cr–Mo and Ni–Cr–Mo–W alloys resistant to uniform, localized corrosion and stress corrosion cracking. Despite an excellent uniform corrosion of Ni–Cr–Mo (W) alloys in both reducing and oxidizing environments, there remains a concern that these alloys could fail due to crevice corrosion in aggressive chloride solutions at high temperatures in a crevice setup [6–10, 14–22, 24]. Table 3 shows the critical pitting temperature (CPT) and critical crevice temperature (CCT) of a wide range of Ni-based alloys and 316L stainless steel obtained using ASTM G-48 test methodology [23]. ASTM G-48 is a standard technique utilized by researchers to determine the materials susceptibility to localized corrosion. The pitting resistance equivalent ($\text{PRE}_{\text{N,W}}$) [31] numbers obtained for the studied alloys are also reported in Table 3.

The CPT and CCT data, obtained for a wide range of alloys, show that an alloy containing optimum amount of Cr (above 20 wt%) and high amount of Mo exhibit the highest localized corrosion resistance. Among the studied

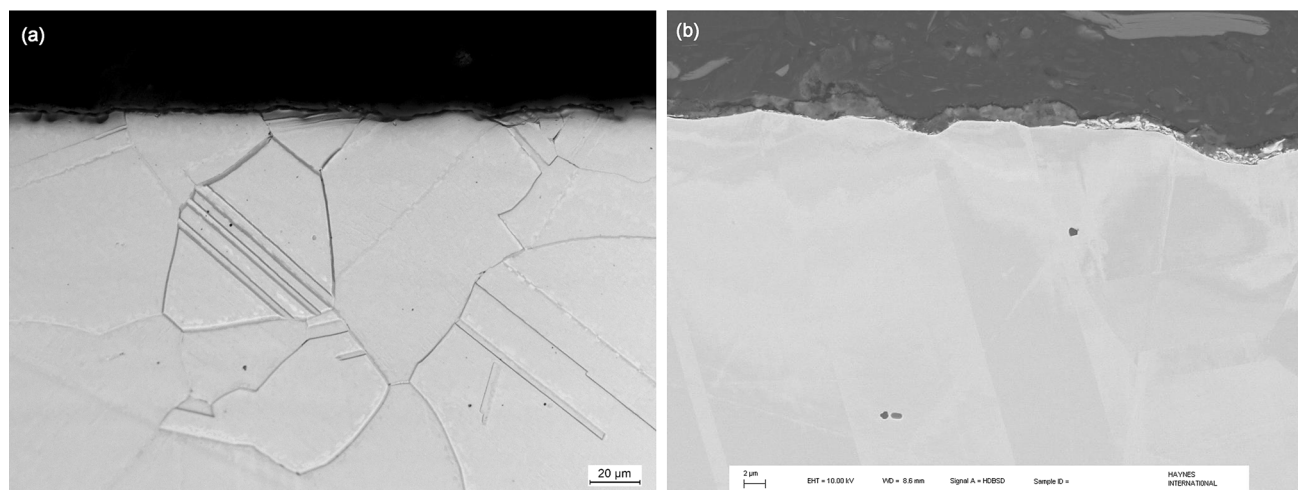


Fig. 20 Microstructures of C-2000 alloy after corrosion testing in 80% H_2SO_4 at 107 °C, **a** optical micrograph and **b** SEM image. EDX spot analysis did not show any enrichment of Mo (or its oxides) in the surface layer

Table 3 Critical pitting temperature (CPT) and critical crevice temperature (CCT) for various alloys obtained using ASTM G-48C, D test methodology ($\text{PRE}_{\text{N,W}}: \% \text{Cr} + 3.3 (\% \text{Mo} + 0.5 \% \text{W}) + 16 \% \text{N}$) [31]

Alloys	CPT (°C)	CCT (°C)	$\text{PRE}_{\text{N,W}}$
316L SS	15	0	28
Alloy 718	45	10	28
Alloy 625	85	35	51
G-35	95	45	59
C-276	>130	55	75
C-22	>130	80	70
C-2000	>130	80	76
C-22HS	>130	100	77

alloys for localized corrosion performance, C-22HS containing 21% Cr and 17% Mo has the highest localized corrosion resistance. In a recent study, Mishra and Shoemsmith [7] investigated the effects of Cr, Mo and W, on the crevice corrosion of a number of commercial Ni–Cr–Mo (W) alloys in sodium chloride solution using conservative electrochemical techniques [20]. It was concluded that Cr is the key element determining resistance to crevice initiation and Mo is the major element controlling crevice propagation and repassivation.

Table 3 shows that G-35 alloy containing high Cr but low Mo and C-276 alloy containing high Mo (or Mo + 0.5 W) but low Cr has a relatively lower localized corrosion resistance, whereas C-22, C-2000 and C-22HS alloys show a significantly higher localized corrosion resistance compared to stainless steel or Ni-based alloys (having low Cr–high Mo or high Cr–low Mo combination). Table 3 also reports the $\text{PRE}_{\text{N,W}}$ number, for various alloys, which is extensively used by the industrial

researchers to predict the materials localized corrosion resistance performance. However, it should be noted that PRE number is just an empirical value. For example, PRE number for C-22 is lower than that for C-276 alloy, but the localized corrosion resistance of C-22 is much higher than that of C-276 alloy (Table 3). Therefore, to exhibit high localized corrosion resistance, an alloy must contain high amount of Cr as well as high Mo (or Mo + W) content.

Summing up, a corrosion-resistant alloy containing high Cr will experience low uniform corrosion in oxidizing solutions, whereas, to obtain a significantly high uniform corrosion resistance in strong reducing acids (like HCl, H_2SO_4), an alloy must contain high amount of Mo (or Mo + W). From the localized corrosion performance, a better choice of material is one which contains high amount of Cr as well as high amount of Mo (or Mo + W). The present study demonstrates that by understanding the role of alloying elements and solution chemistry, the list of materials for application in an aggressive environment can be reduced to few from hundreds of available commercial corrosion-resistant alloys. Nevertheless, there are many other factors (like corrosion performance of welds, material's thermal stability, mechanical performance of materials and cost) which must be considered during the materials selection process.

4 Conclusions

1. Ni-based alloys containing high Mo (like B-3, HYBRID-BC1) demonstrate the highest corrosion resistance in reagent grade concentrated HCl solutions. In the presence of moderate to high levels of oxidizing impurity (Fe^{3+}), an alloy with a high Cr content (like

C-22, C-22HS, C-2000, alloy 59, alloy 686) is required to maintain a low corrosion rate.

2. G-35 alloy (high Cr–low Mo) can also be considered in HCl solution containing high level of oxidants; however, the localized corrosion resistance of G-35 is relatively lower than that of many other Ni–Cr–Mo (W) alloys that must be taken into consideration during materials selection.
3. At free corroding potential, the surface oxide which provides protection against corrosion in concentrated HCl acid is enriched in Mo (or Mo + W).
4. Similar to HCl acid, an alloy containing high Mo (like B-3, HYBRID-BC1) exhibits the highest corrosion resistance in reagent grade concentrated H₂SO₄ solutions. In case, the solution contains moderate to high amount of oxidants, and then, a better choice of material would be one which contain high Cr (like C-22, C-22HS, C-2000, alloy 59, alloy 686).
5. Among C alloys, C-2000 alloy containing Cu demonstrates the highest uniform corrosion resistance in reagent grade H₂SO₄ acid (with and without the presence of oxidants).
6. No noticeable changes in the reducing nature of H₂SO₄ acid were observed at high concentrations, which is a deviation from the previous studies. The present study suggested that an alloy containing high Mo (like B-3, HYBRID-BC1) demonstrates a higher corrosion resistance at high concentrations of H₂SO₄ acid too.
7. It is expected that the oxides of Mo (Mo + W) provide protection to the surface in reagent grade H₂SO₄ acid, similar to HCl acid. Further research work is needed to evaluate the oxide film composition, of materials exposed to H₂SO₄ acid, using surface-sensitive techniques (like XPS, AES).
8. The crevice corrosion resistance of C-22HS alloy, containing optimum amount of Cr and high Mo, is the highest among the studied alloys. Among C alloys, C-22 and C-2000 alloy also demonstrate a high localized corrosion resistance.
9. PRE number is simply an empirical value which assist, to a certain extent, in choosing a right set of alloys. However, prediction of localized corrosion resistance of a material must not be based on its PRE number only.
10. Although the laboratory data provide a good source of information to end users for their initial choice of materials, the actual alloy for an application should be made on the basis of field testing.

Acknowledgements The author acknowledges the efforts of Corrosion technician Ryan Markley and Jeff Dillman from Haynes International (US) in conducting the corrosion tests and Surface Science Western (SSW) at Western University, Canada, for the XPS study.

The author also acknowledges Dr. Paul Crook and Dr. Paul Manning from Haynes International for technical discussion.

References

- [1] MTI Publication MS-1, Materials Selector for Hazardous Chemicals—Sulfuric Acid, Materials Technology Institute of the Chemical Process Industries Inc., 1997, ed. by C.P. Dillon
- [2] MTI Publication MS-3, Materials Selector for Hazardous Chemicals—Hydrochloric Acid, Hydrogen Chloride and Chlorine, Materials Technology Institute of the Chemical Process Industries Inc., 1999, ed. by C.P. Dillon and W.I. Pollock
- [3] W.Z. Friend, *Corrosion of Nickel and Nickel-Based Alloys* (Wiley, New York, 1980), p. 292
- [4] P. Crook, *ASM Handbook*, vol. 13B (ASM International, Materials Park, 2005), p. 228
- [5] A.C. Lloyd, J.J. Noel, S. McIntyre, D.W. Shoesmith, *Electrochim. Acta* **49**, 3015 (2004)
- [6] P. Jakupi, F. Wang, J.J. Noel, D.W. Shoesmith, *Corros. Sci.* **53**, 1670 (2011)
- [7] A.K. Mishra, D.W. Shoesmith, *Corrosion* **70**, 721 (2014)
- [8] J.R. Hayes, J.J. Gray, A.W. Szmodis, C.A. Orme, *Corrosion* **62**, 491 (2006)
- [9] N.S. Meck, P. Crook, D.L. Klarstrom, NACE Corrosion Conference 2004, paper no. 04430 (NACE International, Houston TX, 2004)
- [10] A.K. Mishra, D.W. Shoesmith, P.E. Manning, *Corrosion* (2016). doi:10.5006/2193
- [11] M. Moriya, M.B. Ives, *Corrosion* **40**, 62 (1984)
- [12] M. Moriya, M.B. Ives, *Corrosion* **40**, 105 (1984)
- [13] R. Qvarfort, *Corros. Sci.* **40**, 215 (1998)
- [14] K.J. Evans, A. Yilmaz, S.D. Day, L.L. Wong, J.C. Estill, R.B. Rebak, *J. Met.* **57**, 56 (2005)
- [15] X. Shan, J.H. Payer, *J. Electrochem. Soc.* **156**, C313 (2009)
- [16] N.S. Zadorozne, C.M. Giordano, M.A. Rodriguez, R.M. Carranza, R.B. Rebak, *Electrochim. Acta* **76**, 94 (2012)
- [17] M.A. Rodriguez, R.M. Carranza, R.B. Rebak, *Corrosion* **66**, 1 (2010)
- [18] M.R. Ortiz, M.A. Rodriguez, R.M. Carranza, R.B. Rebak, *Corros. Sci.* **68**, 72 (2013)
- [19] C.M. Giordano, M.R. Ortiz, M.A. Rodriguez, R.M. Carranza, R.B. Rebak, *Corros. Engi. Sci. Technol.* **46**, 129 (2011)
- [20] A.K. Mishra, G.S. Frankel, *Corrosion* **64**, 836 (2008)
- [21] P. Jakupi, J.J. Noel, D.W. Shoesmith, *Corros. Sci.* **54**, 260 (2012)
- [22] N. Ebrahimi, P. Jakupi, J.J. Noel, D.W. Shoesmith, *Corrosion* **71**, 1441 (2015)
- [23] ASTM Annual Book of Standards, Volume 03.02 Wear and Erosion, Metal Corrosion (West Conshohocken, PA) (2011)
- [24] A.K. Mishra, X. Zhang, D.W. Shoesmith, *Corrosion* **72**, 357 (2016)
- [25] N. Sridhar, *Mater. Perform.* **27**, 40 (1988)
- [26] P. Crook, NACE Corrosion Conference 1996, paper no. 412 (NACE International, Houston TX, 1996)
- [27] P. Crook, M.L. Caruso, D.A. Kingseed, *Mater. Perform.* **36**, 49 (1997)
- [28] N. Sridhar, NACE Corrosion Conference 1987, paper no. 19 (NACE International, Houston TX, 1987)
- [29] E.L. Hibner, L.E. Shoemaker, NACE Corrosion Conference 2006, paper no. 6225 (NACE International, Houston TX, 2006)
- [30] G.S. Frankel, *J. Electrochem. Soc.* **145**, 21 (1998)
- [31] Z. Szklarska-Smialowska, *Pitting and Crevice Corrosion of Metals* (Houston, TX, NACE International, 2005)